Detection of Respiration-Induced Field Modulations in fMRI: A Concurrent and Navigator-Free Approach

Alexander Jaffray[1], Christian Kames[1], Michelle Medina[1], Adam Clansey[2], and Alexander Rauscher[2,3,4]

[1]Department of Physics, University of British Columbia, Vancouver, BC, Canada

[2]Department of Mechanical Engineering, University of British Columbia, Vancouver, BC, Canada

[3]Department of Pediatrics, University of British Columbia, Vancouver, BC, Canada

[4]Department of Radiology, University of British Columbia, Vancouver, BC, Canada

Author Information:

Email: ajaffray@physics.ubc.ca

Address: Purdy Pavilion, Room G33, 2211 Wesbrook Mall

Abstract

Functional Magnetic Resonance Imaging (fMRI) is typically acquired using gradient-echo sequences with a long echo time at high temporal resolution. Gradient-echo sequences inherently encode information about the magnetic field in the oft-discarded image phase. We demonstrate a method for processing the phase of reconstructed fMRI data to isolate temporal fluctuations in the harmonic fields associated with respiration by solving a blind source separation problem. The fMRI-derived field fluctuations are shown to be in strong agreement with breathing belt data acquired during the same scan. This work presents a concurrent, hardware free measurement of respiration-induced field fluctuations, providing a respiratory regressor for fMRI analysis which is independent of local contrast changes, and with potential applications in image reconstruction and fMRI analysis.

Introduction

Functional magnetic resonance imaging (fMRI) images time-varying fluctuations in MRI signal associated with changes in blood oxygenation and blood oxygenation level dependent (BOLD) contrast.[1] It is used to identify and map regions of increased and decreased blood oxygenation across the brain, which have been correlated with brain function.[2] Its popularity has led it to become commonplace in medical imaging research investigating brain function at rest and in response to stimulus, under a variety of conditions and states. For BOLD fMRI, data are usually acquired with a T2*-weighted single-shot echo-planar scan. Neural activity causes a local increase in cerebral blood flow (CBF). Due to the resulting increase in venous blood oxygenation, veins become less paramagnetic and the field inhomogeneities around the vessels decrease.[3] Consequently, the loss of signal coherence in the vicinity of blood vessels is slowed down, resulting in an increase in the T2* weighted signal.[1] Changes in CBF are not only due to

neural activity, for example blood CO_2 acts as a strong vasodilator. Adding 5% CO_2 to the inhaled air or oxygen causes an increase in CBF by around 50%.[3] With the brain's oxygen demand remaining unchanged, the venous blood oxygenation increases, even in the absence of neural activity.

Fluctuations in blood CO_2 also occur due to variations in the depth and frequency of breathing, which have a direct influence on cerebral blood flow and consequently influence the BOLD signal in the fMRI scan.[4] A breath hold of 30 seconds, for instance, was shown to increase the BOLD signal by 3-5%.[5] Regular respiratory frequency is around 0.2 to 0.4 Hz, with deep breaths occurring at a rate of 0.05-0.15 Hz.[6] Low-frequency fluctuations are particularly problematic in resting state fMRI (rs-fMRI), as this technique infers functional connections within the brain from correlations in low frequency fluctuations in the BOLD signal, which are in the range of 0.1 Hz.[7] End tidal fluctuations in CO_2 occur at around 0.05 Hz and are correlated with BOLD fMRI signal fluctuations.[8] Birn and colleagues found that respiration depth varied by 19.1% +/- 8.6% during a lexical task and by 17.9% +/- 4.2% when subjects were cued to breath at a constant rate and these changes were significantly correlated to BOLD signal changes.[9]

Respiratory information can be used to model respiratory contributions to the fMRI signal. Regressing out breathing fluctuations during fMRI analysis requires a respiratory measure. External monitoring of respiration using a breathing belt remains the gold standard, and robust methods have been developed to use the measurements from such sensors to remove noise from fMRI acquisitions.[10,11] Power et al. analyzed 440 rs-fMRI scans from the Human Connectome Project data set and found a wide variety of intra- and inter-subject breathing periodicity.[6,12] They observed that over the 14.4. min scan, respiratory rate decreased along with depth of breathing, whereas the variance increased.[6]

At its core, the acquisition of fMRI data utilizes single-shot gradient echo (GRE) echo-planar imaging (EPI) sequences, acquiring relatively low spatial resolution images at high temporal resolutions.[1,13] The signal evolution in a GRE sequence is described by a tissue-specific exponential decay with time constant T_2, and thus contrast within the image is determined by the echo time (TE). In addition to the exponential decay of the signal, voxels in the complex-valued reconstructed image acquire a phase which accumulates with TE and scales with the local resonant frequency offset from the main magnet field B_0.[14,15] The local field offset is determined by the distribution of magnetic susceptibility within and outside of the reconstructed image, and as such, GRE sequences are widely used as input to processing techniques including quantitative susceptibility mapping (QSM) and susceptibility weighted imaging (SWI).[14–17] These image processing techniques use the information about the local magnetic field encoded in the image phase to quantify the local susceptibility distribution and enhance the depiction of vasculature.[18,19]

Considering the phase, each reconstructed fMRI volume is a complex valued depiction of the magnetization sampled at the echo time (TE). It has been shown that respiration induces changes in the magnetic field inside the brain of between 2-5 Hz (approximately 0.01ppm), contributing to physiological noise in the fMRI measurement.[20,21] This field fluctuation amplitude is within the sensitivity range of phase processing routines employed in QSM.[22] Local changes in susceptibility have been observed by processing the phase of fMRI acquisitions in an approach known as functional QSM, an emerging technique which provides motivation for the observability of small field fluctuations in the fMRI scan.[23] While QSM is sensitive to changes in local susceptibility, the measured phase contains contributions from both the local tissue fields and the harmonic background field, which can confound the measurement of susceptibility values in the volume of interest. It is necessary in QSM to subtract the background field to isolate the local susceptibility distribution.[24] One of the useful properties of the background field is that it is harmonic and therefore does not contain contributions from signals within the imaging volume. For the fMRI scan, this means that any temporal changes in the harmonic field must comprise field changes which are independent of the BOLD signal.

Although temporal fluctuations in the harmonic field are independent of BOLD contrast, they cannot be attributed to a specific source of physiological noise without additional constraints. In this work, the identification of harmonic field fluctuations which result from respiratory motion is approached using a blind source separation (BSS) strategy.[25] BSS attempts to isolate signals from multiple sources which have been measured with a single channel. In the case of respiratory field estimation, the fluctuations in the background field are a superposition of a set of fields arising from different susceptibility distributions in the imaging environment and their behavior.

We can model susceptibility sources as dipoles, which have a magnetic field which decays with the cube of the distance from the dipole $B(r) \propto \frac{1}{r^3}$, and so any harmonic field existing within the imaging volume is attributable to nearby susceptibility sources. In the case of fMRI and neuroimaging, this is the body tissue, which is relatively static during the imaging protocol and finite in extent, with motion that can be well-described by a small number of terms.[26] Using a truncated singular value decomposition (SVD), a small set of spatial basis functions and time-varying coefficient vectors can be found which approximate the spatiotemporal evolution of the harmonic field.

We propose to process the phase of fMRI sequences to capture respiration-induced changes in the harmonic field within the imaging volume. The time-course of the harmonic field is approximated using SVD to separate breathing-induced field modulations from other sources of noise.[27] The resulting field modulation can be further projected onto the set of solid harmonic

basis functions, which are used to describe the field fluctuations during acquisition that stem from respiration.

Methods

We acquired a set of 10 fMRI scans in 7 healthy volunteers (weight: 79.7 +/- 12.3 kg, height: 1.80 +/- 0.08 m) at 3T (Philips Elition) using a gradient-echo EPI sequence (duration ~5 minutes) with a SENSE reconstruction (R = 4) and TR/TE of 1150/30. An isotropic voxel size of 2.5 mm and a multi-band factor of 3 was employed to achieve a short TR.[28] Complex data were exported at the console. The size of the reconstructed data was 96×96×57×260 corresponding to 3 spatial dimensions and one temporal dimension. No zero-filling or partial Fourier acquisition was performed.

Respiration of the subjects was monitored using the scanner's respiratory physiology sensor (500Hz sampling rate, positioned around lower chest). One subject was instructed to perform a series of controlled breathing patterns during the scan: A)10 short breaths B) 10 deep breaths, C) free-breathing, D) breath-hold of 10 to 20 s. All other subjects were given no specific instructions regarding respiration.

After acquisition, the resting-state fMRI data was sliced along the temporal dimension to produce 260 volumes which were individually processed (Figure 1) using the following steps: Laplacian-based phase unwrapping was performed to remove phase discontinuities in the image.[29] The local field was estimated from the unwrapped phase with regularized SHARP.[24] Then, the background harmonic field was estimated by subtracting the local field from the total field.

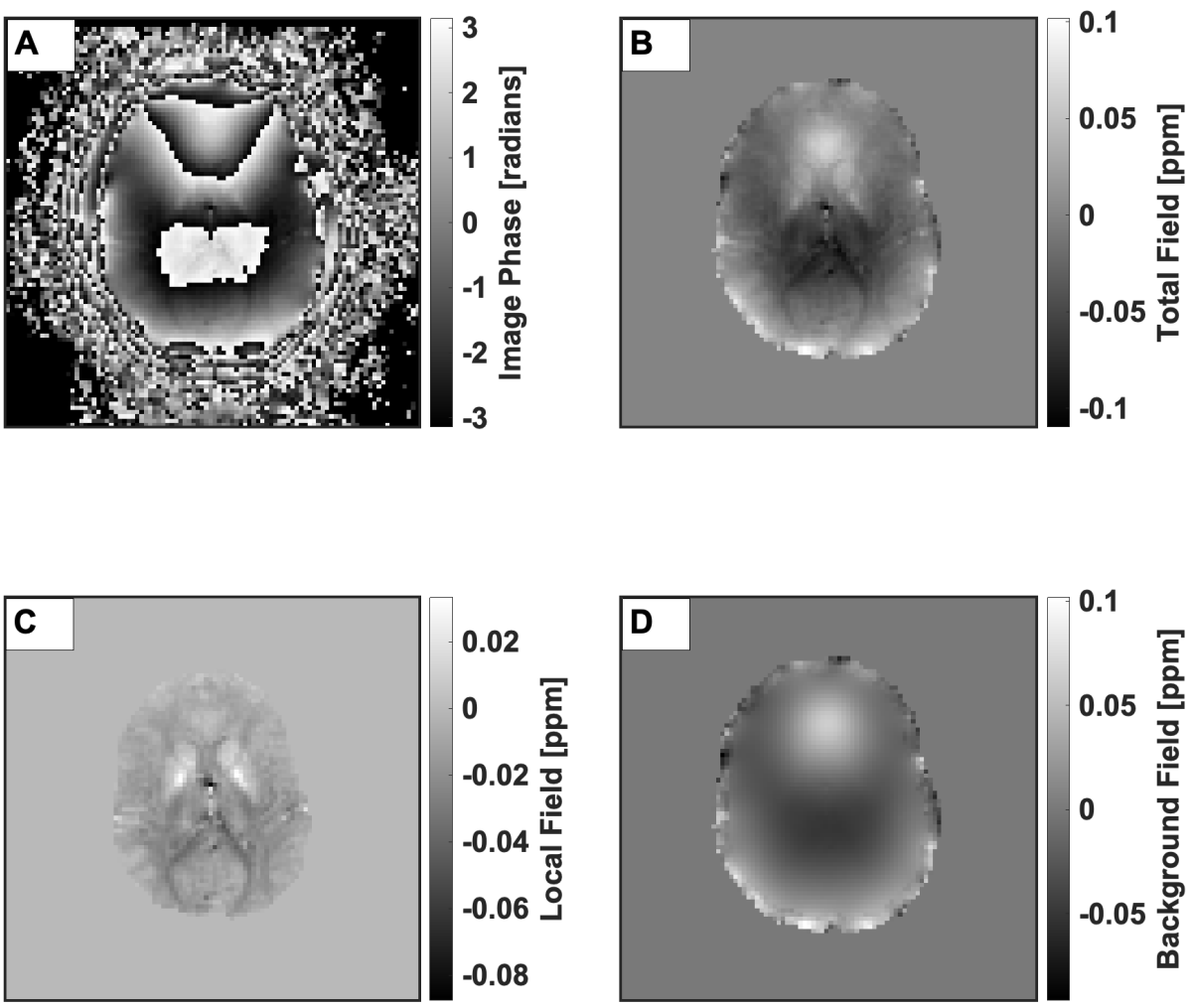

Figure 1: Illustration of the pipeline from raw image phase to harmonic background field. All images are of a single slice taken from the first timepoint of the fMRI time-series. (A) Raw image phase. (B) Image phase after unwrapping with Laplacian unwrapping. (C) The projection of the total field onto the local susceptibility sources within the volume of interest. Note the absence of low-frequency phase modulation across the slice. (D) The isolated harmonic field, obtained by subtraction of the local field in (C) from the total field depicted in (B).

The estimated harmonic field data from all volumes was reshaped into a MxN matrix P where M is the number of spatial voxels and N is the number of time samples during the acquisition. The field was then decomposed using Singular-Value Decomposition (SVD) and a temporally low-rank representation of the background field was reconstructed by truncating the diagonal of the matrix S to obtain S_L.[30]

Discrimination of the harmonic field component corresponding to respiration $v_r(t)$ was performed by finding the right singular vector $v_i(t): i \in [1,5]$ of the low-rank representation P_L with the maximal instantaneous variation. This was accomplished by defining $v_r(t)$ to be the $v_i(t)$ for which $|\frac{dv_i}{dt}|$ was maximized. A visualization of the separated harmonic field components is shown for an arbitrary region of interest in Figure 2.

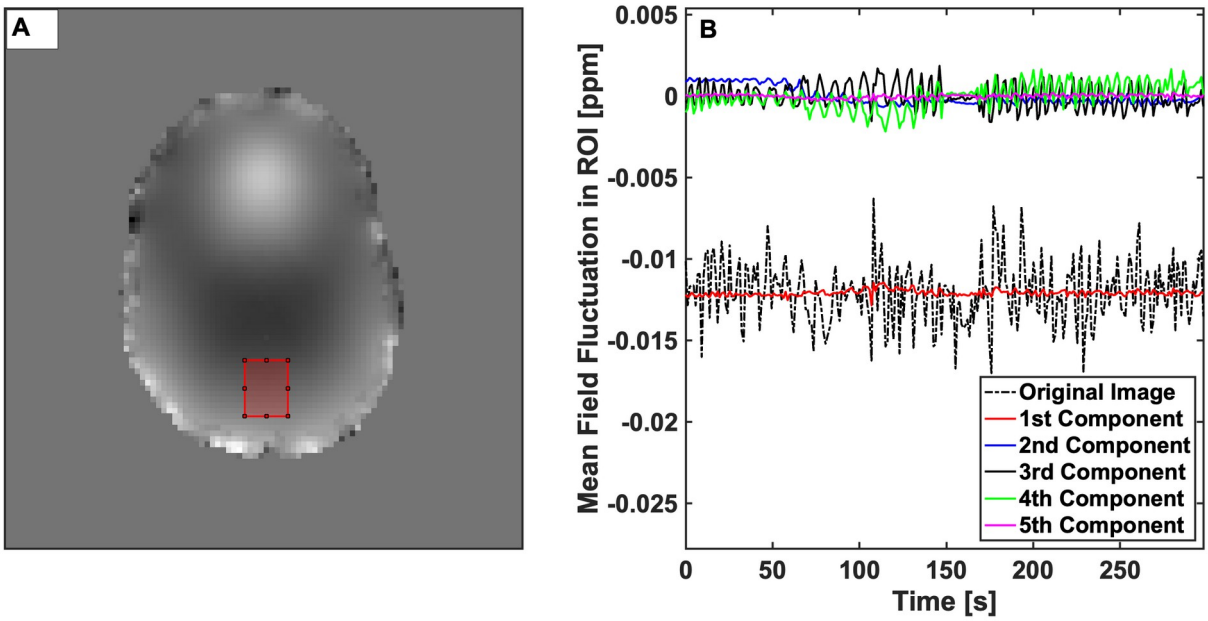

Figure 2: Separation of the 5 dominant time-varying contributions to the field evolution within an example region of interest, depicted in red in (A). (B) Time-varying magnetic field within the region of interest shown as a dashed line. The coloured lines show the first 5 right singular vectors in the time domain, which sum to the raw field evolution (dashed). The black (third) component is clearly periodic and contains most of the temporal variation in the measured magnetic field.

After discrimination of the correct $v_r(t)$, the resulting field estimated from $v_r(t)$ at each timepoint was projected onto the set of solid harmonics (up to third order) to produce a matrix of solid harmonic coefficients which describes the time evolution of the respiration-induced field modulation. The zeroth coefficient was chosen as the respiratory regressor for comparison with the breathing belt measurement. Pseudocode for the proposed method is given in Algorithm 1. Processing of the data was performed in MATLAB and took 150s on a 32-core workstation.

Algorithm 1: Respiration-Induced Field Estimation

Data: D : Complex 4D fMRI Data
Result: F : Solid Harmonic Coefficients
`/* Process Raw Complex Data */`
$\Phi \leftarrow \text{unwrap}(\phi(D))$;
$\Phi' \leftarrow \text{highpass}(\Phi)$;
$\Phi_0 \leftarrow \Phi - \Phi'$;

`/* Reshape and Decompose */`
$N_x, N_y, N_z, N_t \leftarrow \text{size}(\Phi_0)$;
$P \leftarrow \text{reshape}(\Phi_0, N_x \times N_y \times N_z, N_t)$;
$USV^T \leftarrow \text{svd}(P)$;

`/* Find Field Component with Maximal Instantaneous Variation */`
$v_r \leftarrow [\,]$;
$\kappa \leftarrow 0$;
$l \leftarrow 0$;
while $i \leq 5$ **do**
  $v_i \leftarrow V[:, i]$;
  if $|\frac{dv_i}{dt}|_1 \geq \kappa$ **then**
    $v_r \leftarrow v_i$;
    $\kappa \leftarrow |\frac{dv_i}{dt}|_1$;
    $l \leftarrow i$
  end
  $i \leftarrow i + 1$;
end
$S_L \leftarrow \text{zeros}(\text{size}(S))$;
$S_L[l, l] \leftarrow S[l, l]$;
$P_L \leftarrow US_LV^T$;

`/* Fit Solid Harmonics to Maximally Varying Field */`
$F \leftarrow \text{fitSolidHarmonics}(P_L; \text{order} = 3)$;

Algorithm 1: Pseudocode outlining the proposed method.

Processing of the breathing-belt respiratory trace was also performed in MATLAB using standard tools available in the PhysIO toolbox.[11] The trace was lowpass filtered and de-spiked to remove spurious noise. The breathing-belt respiratory trace was sampled at approximately 500 Hz, while the field evolution derived using the proposed method was sampled every volume TR (1150 ms, or 0.87 Hz). An offset correction step was performed to ensure that recorded sampling times for both measurements were synchronized. The temporal evolution of the field modulations measured using the proposed method was compared to the breathing-belt respiratory trace by measuring the error in respiratory period and peak/trough locations between

the signals. As well, visual comparison of the respiratory trace and the field modulations was performed for all subjects, and the timepoints associated with breathing pattern changes were observed and compared with the instructions given to the control subject.

Synthesis of respiratory phase was performed for the control subject using a histogram-based method proposed for RETROICOR, and applied to both the zeroth order field modulation and the respiratory sensor signal.[10] The reference respiratory phase and the respiratory phase obtained from the proposed method were compared by measuring the error in respiratory period and peak/trough locations.

Results

Measured field modulations correlated strongly with the respiratory trace obtained from the breathing belt for all subjects. Correspondence with the reference respiratory phase was maintained across shallow, deep, and free-breathing periods, and for the range of respiratory frequencies observed across the subject cohort (Figure 3). Peaks of the respiration-induced field modulation were well-resolved, with no obvious aliasing in the reconstructed coefficient vectors. For the control subject, distinct periods of controlled breathing were seen that corresponded directly with subject instruction. The root mean-square error in the measured respiratory period was 0.3 s between the ground-truth and proposed method for the control subject.

The overlap in detected peaks across trace obtained with the proposed method and the breathing belt trace was 94% over all scans. Across all subjects, the root mean-square error in measured respiratory period between the ground-truth and the proposed method was 0.68 seconds or 17% of the average respiratory period, and the mean absolute error was 0.51 seconds. The mean error in peak locations between the ground-truth and proposed method was 0.57 seconds. The group mean of the respiratory period (4.79 +/- 1.6 seconds) measured across all subjects using the proposed method was congruent with that measured with the breathing belt to 3 significant digits.

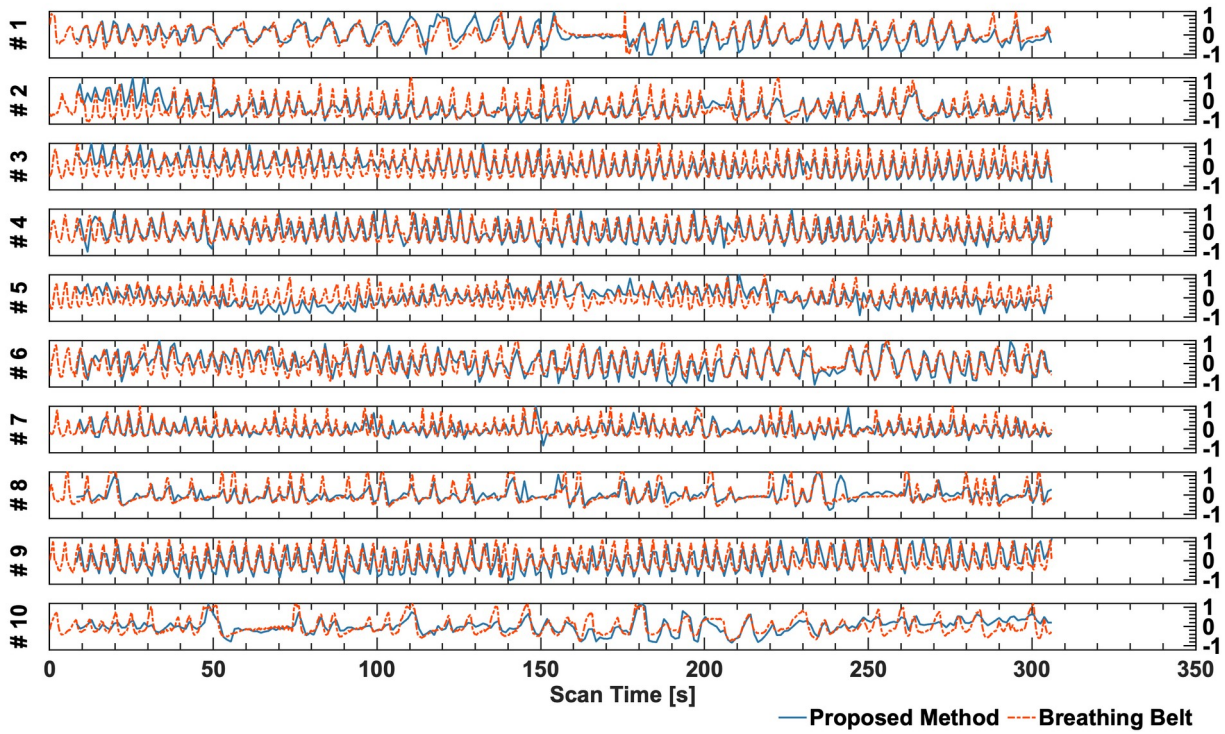

Figure 3: Respiration induced zeroth order field modulation derived from fMRI time-series data using the proposed method (blue) and normalized externally monitored respiratory trace (red, dashed) for all subjects. Strong agreement is shown between both the proposed method and the externally monitored respiratory trace.

The spectrum of singular values (Figure 4) obtained from the SVD of P was consistent with the assumption that fluctuations in the harmonic field were low rank, indicating that P_L was a good approximation of P. Isolation of the $v_i(t)$ corresponding to respiration was reliably performed using our method. The L_1-norm distribution of the derivatives of the columns of V was found to be consistently dominated by one component for all subjects and was not biased towards the component associated with the largest singular value of P.

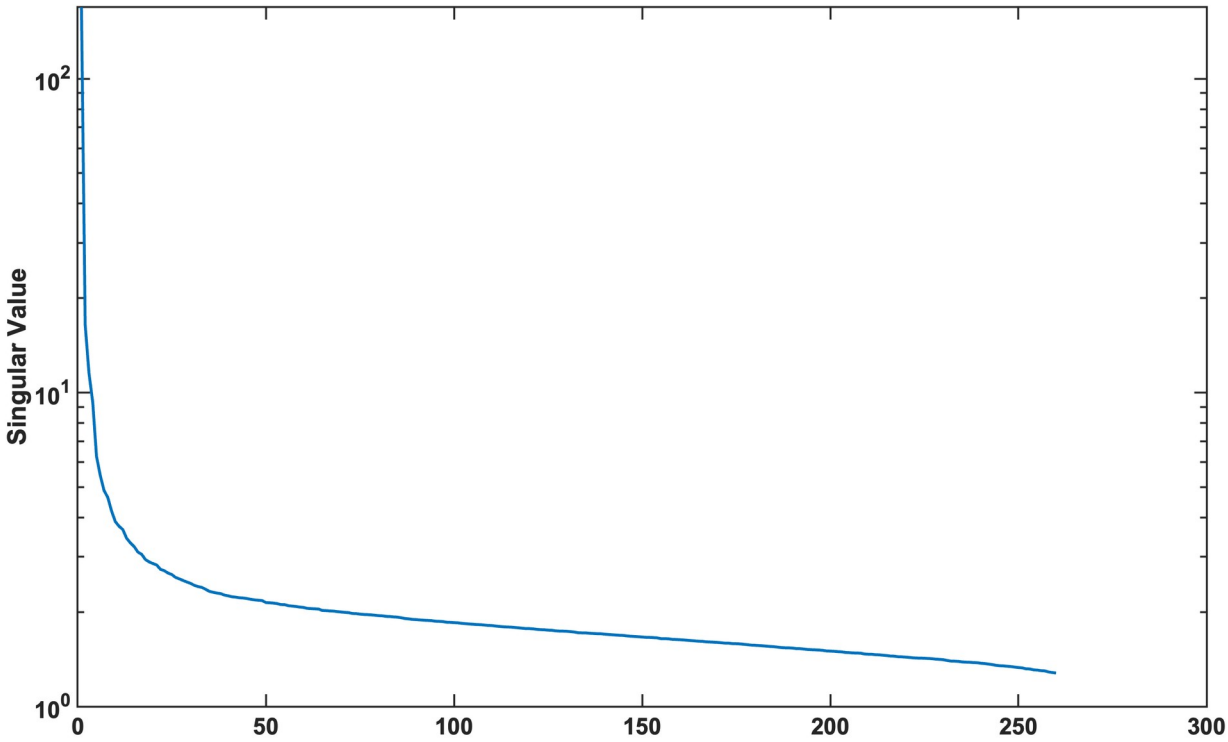

Figure 4: Singular values of the matrix P demonstrating significant decay beyond the first 5 singular values. The first 5 singular vectors describe 97% of the variance in the data, validating the assumption in the proposed work that the matrix P can be well-characterized by a low-rank approximation.

Determination of the solid harmonic coefficients describing the temporal and spatial behavior of the respiration-induced field during respiration was possible in all subjects, and the solid harmonic fitting procedure did not result in significant spurious coefficient values across the whole scan duration. This is seen in Figure 5, where the patterns of controlled breathing are evident in all solid harmonic basis function coefficients.

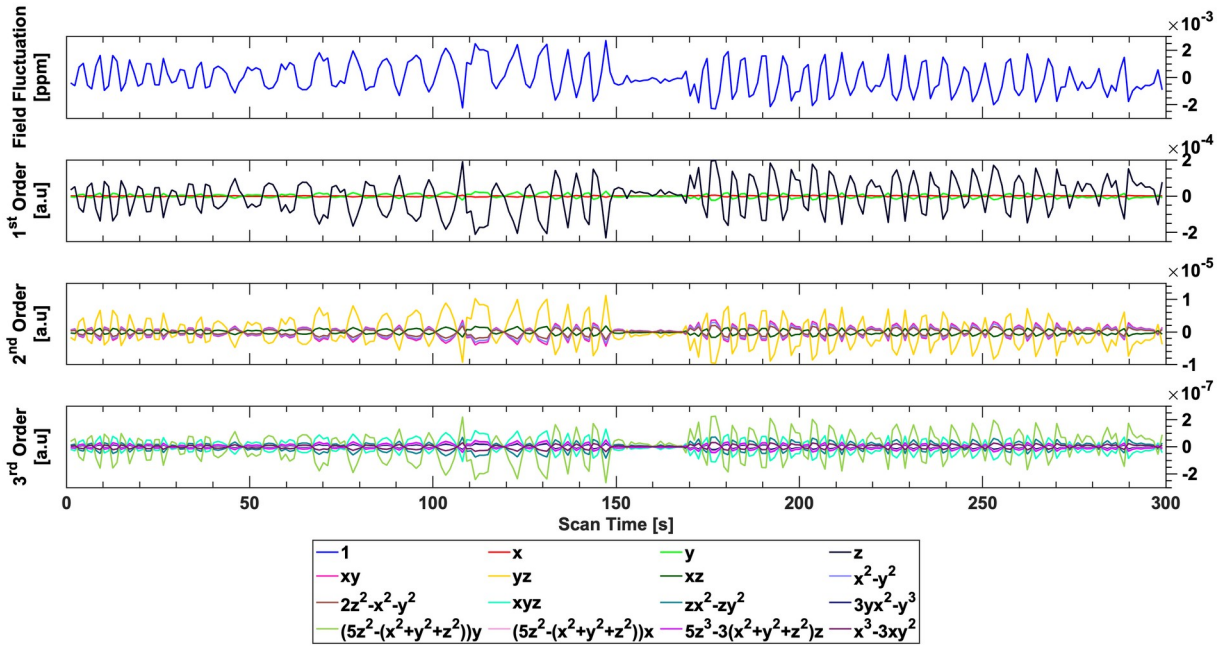

Figure 5: Projection of the temporal evolution of the field onto solid harmonics (see legend for definition) for the control subject, obtained using the proposed method. The primary fluctuation observed is in the zeroth order coefficient, however strong correlations are seen across all coefficients, indicating that respiratory induced field fluctuations can likely be described by a single mode. Instructed breathing periods are seen in all coefficients. The zeroth order fluctuations demonstrate a maximal field excursion of 2.5 ppb, however local field excursions due to higher order coefficients can be up to 15 ppb.

Maximal field excursions due to respiration were observed to be between -5 ppb and +15 ppb within the imaged volume for the control subject, which corresponds to an approximate range of 2.2 Hz at 3T, consistent with previous measurement of field perturbations due to breathing.[20,21] The average maximal field excursion over all subjects within the imaging volume was 3.05Hz +/- 1.2Hz. These excursions were most significant in the periphery of the imaging volume, where the higher order terms in the solid harmonic expansion become dominant, as seen in Figure 6.

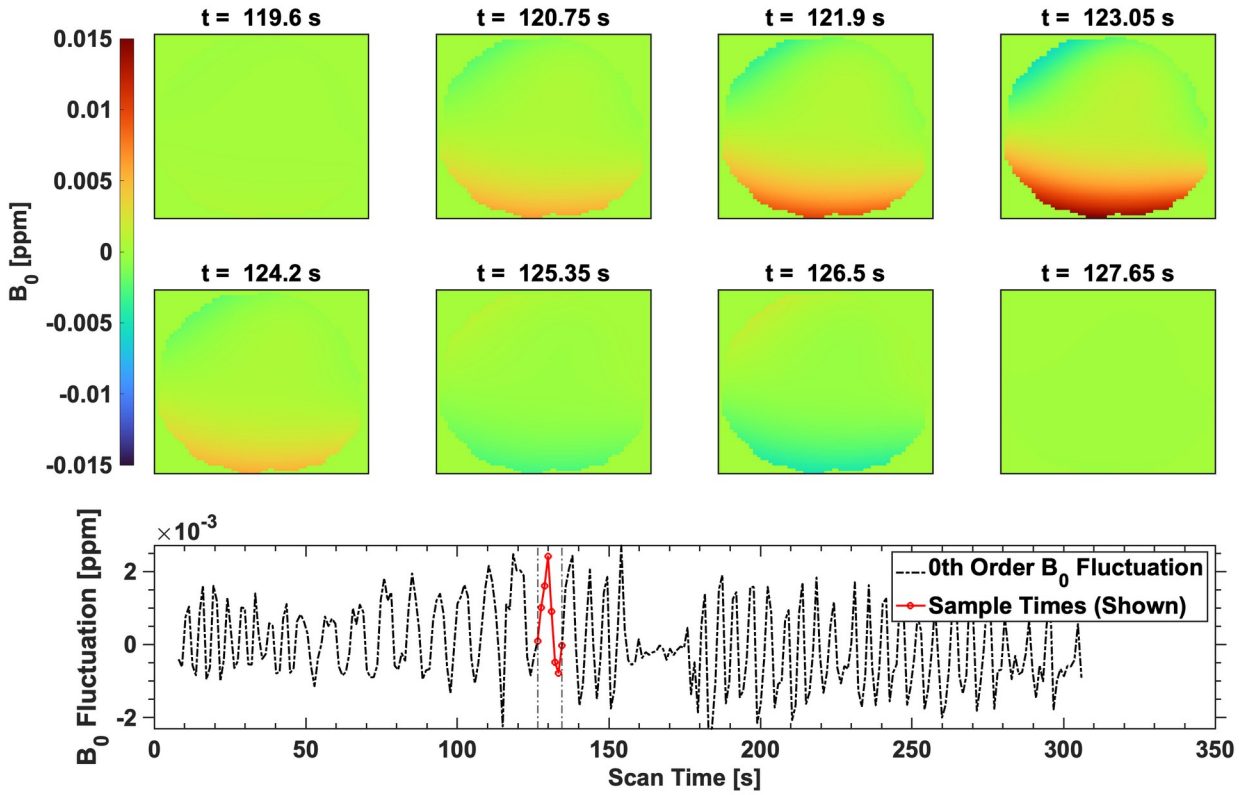

Figure 6: Illustration of the respiration-induced field modulation during a single respiratory period for the control subject. Each image is a masked depiction of the field in the central axial slice of the imaging volume, sampled during the scan at time points indicated in the lower sub-figure. The maximal field excursion over the respiratory period in the imaging volume is [-5 ppb, +15 ppb].

Synthesized respiratory phase from the zeroth order solid harmonic fluctuations agreed strongly with respiratory phase obtained from the breathing belt (Figure 7). Distinct periods of controlled breathing were seen in both synthesized and reference traces that corresponded directly with subject instruction. Peaks of the respiratory phase were well-resolved, with no obvious aliasing in the reconstructed signal. For the control subject, root mean square error between respiratory period measured with the breathing belt and derived from the fMRI acquisition was 0.31 seconds. Correspondence with the reference respiratory phase was maintained across shallow, deep, and free-breathing periods. Respiratory phase was not accurately determined during the free-breathing period using either the proposed method or the physiology sensor.

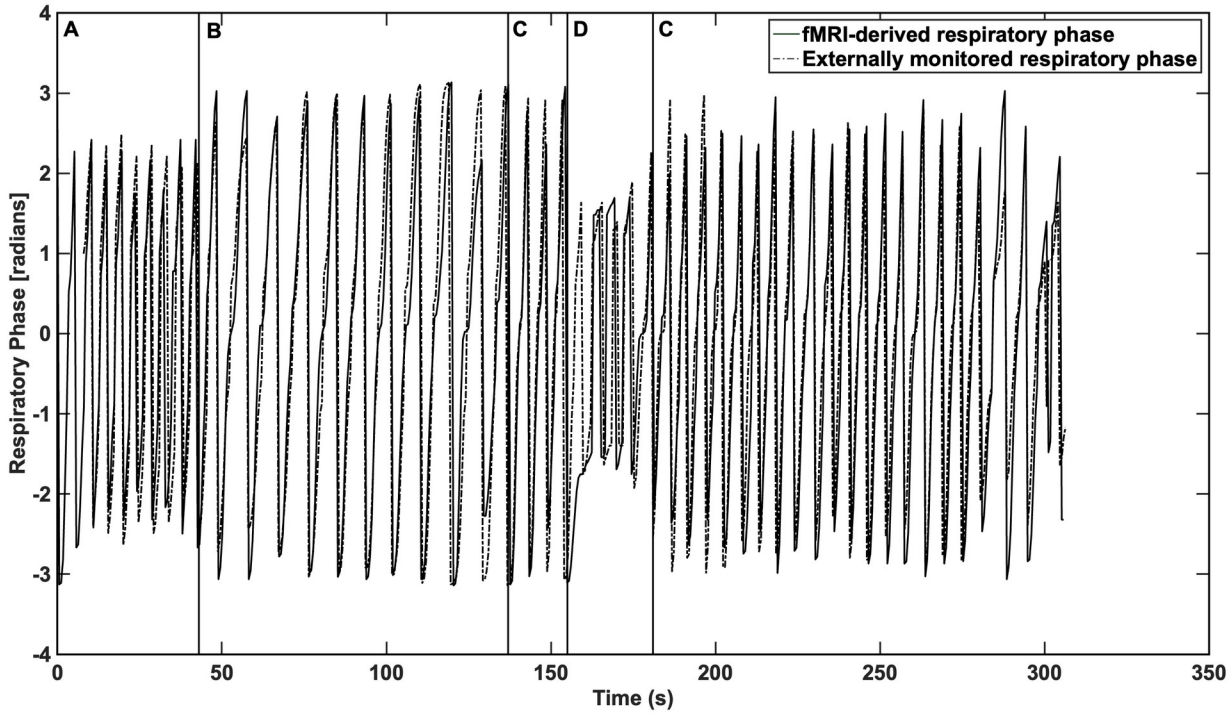

Figure 7: Respiratory phase derived from fMRI time-series data (blue) and externally monitored respiratory phase (dashed). Structured breathing patterns are denoted with the letters A through D. Shallow breathing is denoted with the letter A. Deep, slow breathing is denoted with the letter B. Free breathing is denoted with the letter C. A breath hold was conducted during the period denoted with the letter D. Strong agreement is shown between both the fMRI-derived respiratory phase and the externally monitored respiratory phase, with peak and trough locations showing good correspondence.

Discussion and Conclusion

We demonstrate the feasibility of hardware-free estimation of respiration-induced field modulations from fMRI image data on a cohort of 7 healthy volunteers. The proposed method is robust to scan acceleration and concurrent with the fMRI experiment, requiring no additional or interleaved acquisitions. The method can be applied retrospectively if the image phase is available and facilitates physiological noise correction by providing an independent respiratory regressor in fMRI studies for which external physiology monitoring is not available or corrupted.[6,9,31]

The proposed method was shown to be applicable to subjects with a wide range of respiratory rates, as seen in Figure 3. However, an important limitation is that the TR must be shorter than half of the shortest respiration period, a necessary condition for alias-free respiratory trace reconstruction. While this limitation was not encountered in the scope of the present work, the

proposed method would not be applicable to populations for whom the resting respiratory rate is greater than twice the volume acquisition rate (1/TR). Nevertheless, there is significant effort in fMRI research to increase temporal resolution with novel image acquisition and reconstruction strategies, such as 3D spiral readouts for fMRI.[32–34] These strategies have been demonstrated in vivo with a TR as short as 300 ms for the whole brain volume, which is sufficiently short to adequately sample respiratory fluctuations even in populations with very high respiratory frequency, such as newborns or very young children.

The proposed method is robust to small, non-periodic or low-frequency head motions which result in step changes in the harmonic field in the volume of interest. While the step changes do perturb the harmonic field depiction in the volume of interest, they do not influence the frequency content of the component associated with respiration. They are observed as separate components after performing the SVD and can be clearly seen in the second and 4th component of the decomposition in Figure 2. While field perturbations due to head motion correlated with respiration cannot be filtered out, the images can be registered to minimize apparent head motion. If this is done, any field change due to head motion will be projected onto the harmonic field changes associated with respiration. It is unclear whether this significantly compromises the robustness of the proposed method.

Obtaining breathing information using the fMRI data has several advantages over recording respiration with a belt. Using the belt is prone to errors, for example in obese or small participants. In situations of low chest movement, for example in the case of abdominal breathing, respiration may not be adequately detected. Our results suggest that field fluctuations created by the inflation and deflation of the lungs capture inhalation and exhalation events that the belt misses (see Figure 3). Furthermore, in some populations the belt may be distracting and wearing it may interfere with the fMRI experiment. The breathing information obtained with the proposed method is automatically synchronized with the fMRI experiment and the processing of the data requires no user interaction. The measured error in respiratory period between the ground-truth belt recordings and the proposed method is less than the volume TR of the fMRI scan, and group statistics are identical across both methods. If the fMRI data are usable for fMRI analysis, they are automatically usable for the tracking of breathing, provide the phase information is saved.

The proposed method is physics driven and does not require any training of a network. A drawback is that it cannot be applied retrospectively to existing fMRI scans if phase information is unavailable. In such situations, estimation of breathing using a machine learning (ML) approach that works with the magnitude data was proposed as a solution.[35] The training of the network requires considerable quality assurance and data cleaning by hand, such as the removal of spike artifacts in the breathing belt data. Only about 14% of the data from the Developing Human Connectome Project could be used for training.[35,36] In addition, the same authors

identified 52.1 % of the Young Adult HCP and 18.9% of the Aging HCP breathing data as good quality respiratory signals.[37,38] Power et al. report that any of three measures typically derived from breathing belt data (respiration variation, the envelope of the respiratory trace, and respiratory volume per time) may miss deep breaths.[6] These findings further underline the notion that field fluctuations may be a more reliable measure of breathing than using a belt, especially in pediatric and aging populations. Retrospective application of a machine learning based approach may require the acquisition of additional training data to tune the network to the specific parameters of the fMRI scan. Furthermore, a machine-learning approach which is applied to magnitude data must extract a respiratory regressor from the BOLD time-series, which is the signal of interest in fMRI. This presents the potential for the respiratory regressor to attribute true BOLD contrast fluctuations to respiration, which would be incorrectly removed upon physiological noise correction. While training on a large, augmented dataset can improve generalizability of the ML method, the acquisition of such a dataset can be difficult for some populations, and the possibility of confounding respiratory and true fMRI signals cannot be eliminated.

The choice of basis expansion to describe the field changes during fMRI acquisition was chosen as the set of solid harmonics up to 3rd order, consistent with existing field estimation work, however use of the proposed method for respiratory phase synthesis would only need an expansion of 1st order. Higher temporal resolution field estimation has been reported, with a significant compromise with regards to imaging resolution.[39] However, it may be feasible to extend the proposed method to take advantage of parallel acquisition strategies beyond the reduction in volume TR to significantly increase sampling rate while preserving in-plane resolution. Acquisition strategies which use simultaneous multi-slice encoding sample multiple locations along the slice-select direction at the same time. This would allow for the fitting of solid harmonics at the repetition time of each slice group, presenting an increase in temporal sampling rate by at least an order of magnitude (a factor of 19 in the protocol used in the present work).

Recently, a method for physiological regressor estimation on a slice-TR timescale has been proposed (PREPAIR), which identifies time-series signals from magnitude and phase of the fMRI images and performs power spectrum analysis and filtering to derive both respiratory and cardiac regressors.[40] While this method utilizes the phase of the reconstructed image to aid regressor estimation, it does not comprise estimation of the magnetic field changes due to respiration but uses the phase as a source of physiological noise information. While it has been demonstrated as a robust method for regressor estimation and is notably capable of extracting a cardiac regressor sampled at slice-TR, it does not produce an estimate of the magnetic field during the fMRI acquisition. Furthermore, the regressors obtained from PREPAIR are determined to be independent of the BOLD signal by a filtering process, whereas in the proposed

method the estimated respiratory regressor is constructed to preclude frequency domain filtering and enforce independence to the BOLD signal by physical constraint.

The computational overhead of the proposed method is minimal, only requiring the phase to be saved at the console and exported to a standard imaging format such as DICOM. The phase must be reconstructed regardless of whether it is exported, so no additional reconstruction time would be required during the imaging session. Processing of the exported phase images can be done offline in approximately 2 minutes for the whole fMRI time series of 260 volumes.[41] Standard processing pipelines for fMRI data, such as fMRIprep, already have significant computational overhead, and adding the proposed method as an additional step would not be a disruption to fMRI workflows.[42] The current implementation of the proposed method is available in MATLAB. Implementations of the phase processing algorithms used in this work are part of the open-source QSM toolboxes and are available in MATLAB and Julia programming languages (https://github.com/kamesy/QSM.jl, https://github.com/kamesy/QSM.m). The code to reproduce the results from this paper is available at https://github.com/alexjaffray/fMRI-phase-toolbox and the data is available upon request. The proposed approach is not limited to fMRI but can be employed in all scans that acquire gradient echo data at sufficiently high temporal resolution, such as dynamic susceptibility contrast MRI or measurements of cerebrovascular reactivity.[43–45]

Acknowledgements

All work was conducted at the University of British Columbia, located on the traditional, ancestral and unceded territory of the Musqueam people. AR acknowledges support from Canada Research Chairs (950-230363), the Natural Sciences and Engineering Council of Canada (016-05371), and the Canadian Institutes of Health Research (RN382474-418628 and 479213-MPI-CAAA-18330).

References:

1. Ogawa S, Tank DW, Menon R, et al. Intrinsic signal changes accompanying sensory stimulation: functional brain mapping with magnetic resonance imaging. *Proc Natl Acad Sci*. 1992;89(13):5951-5955. doi:10.1073/pnas.89.13.5951
2. Ogawa S, Lee TM, Stepnoski R, Chen W, Zhu XH, Ugurbil K. An approach to probe some neural systems interaction by functional MRI at neural time scale down to milliseconds. *Proc Natl Acad Sci*. 2000;97(20):11026-11031. doi:10.1073/pnas.97.20.11026
3. Rauscher A, Sedlacik J, Barth M, Haacke EM, R. Reichenbach J. Nonnvasive assessment of vascular architecture and function during modulated blood oxygenation using susceptibility weighted magnetic resonance imaging. *Magn Reson Med*. 2005;54(1):87-95. doi:10.1002/mrm.20520
4. Chang C, Glover GH. Relationship between respiration, end-tidal CO2, and BOLD signals in resting-state fMRI. *NeuroImage*. 2009;47(4):1381-1393. doi:10.1016/j.neuroimage.2009.04.048
5. Kastrup A, Krueger G, Glover GH, Moseley ME. Assessment of cerebral oxidative metabolism with breath holding and fMRI. *Magn Reson Med*. 1999;42(3):608-611. doi:10.1002/(SICI)1522-2594(199909)42:3<608::AID-MRM26>3.0.CO;2-I
6. Power JD, Lynch CJ, Dubin MJ, Silver BM, Martin A, Jones RM. Characteristics of respiratory measures in young adults scanned at rest, including systematic changes and "missed" deep breaths. *NeuroImage*. 2020;204:116234. doi:10.1016/j.neuroimage.2019.116234
7. Biswal B, Yetkin FZ, Haughton VM, Hyde JS. Functional connectivity in the motor cortex of resting human brain using echo-planar MRI. *Magn Reson Med*. 1995;34(4):537-541. doi:10.1002/mrm.1910340409
8. Wise RG, Ide K, Poulin MJ, Tracey I. Resting fluctuations in arterial carbon dioxide induce significant low frequency variations in BOLD signal. *NeuroImage*. 2004;21(4):1652-1664. doi:10.1016/j.neuroimage.2003.11.025
9. Birn RM, Diamond JB, Smith MA, Bandettini PA. Separating respiratory-variation-related fluctuations from neuronal-activity-related fluctuations in fMRI. *NeuroImage*. 2006;31(4):1536-1548. doi:10.1016/j.neuroimage.2006.02.048
10. Glover GH, Li TQ, Ress D. Image-based method for retrospective correction of physiological motion effects in fMRI: RETROICOR. *Magn Reson Med*. 2000;44(1):162-167. doi:10.1002/1522-2594(200007)44:1<162::aid-mrm23>3.0.co;2-e
11. Kasper L, Bollmann S, Diaconescu AO, et al. The PhysIO Toolbox for Modeling Physiological Noise in fMRI Data. *J Neurosci Methods*. 2017;276:56-72. doi:10.1016/j.jneumeth.2016.10.019
12. Van Essen DC, Smith SM, Barch DM, et al. The WU-Minn Human Connectome Project: an overview. *NeuroImage*. 2013;80:62-79. doi:10.1016/j.neuroimage.2013.05.041
13. Glover GH. Overview of Functional Magnetic Resonance Imaging. *Neurosurg Clin N Am*. 2011;22(2):133-139. doi:10.1016/j.nec.2010.11.001
14. Reichenbach JR, Haacke EM. Gradient Echo Imaging. In: Haacke EM, Reichenbach JR, eds. *Susceptibility Weighted Imaging in MRI*. Hoboken, NJ, USA: John Wiley & Sons, Inc.; 2011:33-46. doi:10.1002/9780470905203.ch3

15. Rauscher A, Sedlacik J, Deistung A, Mentzel HJ, Reichenbach JR. Susceptibility Weighted Imaging: Data Acquisition, Image Reconstruction and Clinical Applications. *Z Für Med Phys*. 2006;16(4):240-250. doi:10.1078/0939-3889-00322
16. Wang Y, Liu T. Quantitative susceptibility mapping (QSM): Decoding MRI data for a tissue magnetic biomarker. *Magn Reson Med*. 2015;73(1):82-101. doi:10.1002/mrm.25358
17. Rauscher A, Haacke EM, Neelavalli J, Reichenbach JR. Phase and its Relationship to Imaging Parameters and Susceptibility. In: *Susceptibility Weighted Imaging in MRI*. John Wiley & Sons, Ltd; 2011:47-71. doi:10.1002/9780470905203.ch4
18. Reichenbach JR, Venkatesan R, Schillinger DJ, Kido DK, Haacke EM. Small vessels in the human brain: MR venography with deoxyhemoglobin as an intrinsic contrast agent. *Radiology*. 1997;204(1):272-277. doi:10.1148/radiology.204.1.9205259
19. Ayaz M, Boikov A, McAuley G, et al. Imaging Cerebral Microbleeds with SWI. In: *Susceptibility Weighted Imaging in MRI*. John Wiley & Sons, Ltd; 2011:191-214. doi:10.1002/9780470905203.ch12
20. Van de Moortele PF, Pfeuffer J, Glover GH, Ugurbil K, Hu X. Respiration-induced B0 fluctuations and their spatial distribution in the human brain at 7 Tesla. *Magn Reson Med*. 2002;47(5):888-895. doi:10.1002/mrm.10145
21. Vannesjo SJ, Miller KL, Clare S, Tracey I. Spatiotemporal characterization of breathing-induced B0 field fluctuations in the cervical spinal cord at 7T. *NeuroImage*. 2018;167:191-202. doi:10.1016/j.neuroimage.2017.11.031
22. Deistung A, Schweser F, Reichenbach JR. Overview of quantitative susceptibility mapping: Overview of Quantitative Susceptibility Mapping. *NMR Biomed*. 2017;30(4):e3569. doi:10.1002/nbm.3569
23. Sun H, Seres P, Wilman AH. Structural and functional quantitative susceptibility mapping from standard fMRI studies: QSM from fMRI studies. *NMR Biomed*. 2017;30(4):e3619. doi:10.1002/nbm.3619
24. Sun H, Wilman AH. Background field removal using spherical mean value filtering and Tikhonov regularization. *Magn Reson Med*. 2014;71(3):1151-1157. doi:10.1002/mrm.24765
25. Golub GH, Reinsch C. Singular value decomposition and least squares solutions. *Numer Math*. 1970;14(5):403-420. doi:10.1007/BF02163027
26. Welch EB, Manduca A, Grimm RC, Ward HA, Jr CRJ. Spherical navigator echoes for full 3D rigid body motion measurement in MRI. *Magn Reson Med*. 2002;47(1):32-41. doi:10.1002/mrm.10012
27. Agrawal U, Brown EN, Lewis LD. Model-based physiological noise removal in fast fMRI. *NeuroImage*. 2020;205:116231. doi:10.1016/j.neuroimage.2019.116231
28. Pruessmann KP, Weiger M, Scheidegger MB, Boesiger P. SENSE: Sensitivity encoding for fast MRI. *Magn Reson Med*. 1999;42(5):952-962. doi:10.1002/(SICI)1522-2594(199911)42:5<952::AID-MRM16>3.0.CO;2-S
29. Schofield MA, Zhu Y. Fast phase unwrapping algorithm for interferometric applications. *Opt Lett*. 2003;28(14):1194-1196. doi:10.1364/OL.28.001194
30. Wold S, Esbensen K, Geladi P. Principal component analysis. *Chemom Intell Lab Syst*. 1987;2(1):37-52. doi:10.1016/0169-7439(87)80084-9
31. Golestani AM, Chen JJ. Controlling for the effect of arterial-CO2 fluctuations in resting-state fMRI: Comparing end-tidal CO2 clamping and retroactive CO2 correction. *NeuroImage*. 2020;216:116874. doi:10.1016/j.neuroimage.2020.116874

32. Moeller S, Yacoub E, Olman CA, et al. Multiband multislice GE-EPI at 7 tesla, with 16-fold acceleration using partial parallel imaging with application to high spatial and temporal whole-brain fMRI. *Magn Reson Med*. 2010;63(5):1144-1153.
33. Kasper L, Engel M, Heinzle J, et al. Advances in spiral fMRI: A high-resolution study with single-shot acquisition. *NeuroImage*. 2022;246:118738. doi:10.1016/j.neuroimage.2021.118738
34. Engel M, Kasper L, Patzig F, Bianchi S, Prüssmann, K. Whole-brain fMRI at 5 frames per second using T-Hex spiral acquisition. In: *Proceedings of the International Society for Magnetic Resonance in Medicine (ISMRM) 2021*. Vol 0886.
35. Addeh A, Vega F, Medi PR, Williams RJ, Pike GB, MacDonald ME. Direct machine learning reconstruction of respiratory variation waveforms from resting state fMRI data in a pediatric population. *NeuroImage*. 2023;269:119904. doi:10.1016/j.neuroimage.2023.119904
36. Somerville LH, Bookheimer SY, Buckner RL, et al. The Lifespan Human Connectome Project in Development: A large-scale study of brain connectivity development in 5-21 year olds. *NeuroImage*. 2018;183:456-468. doi:10.1016/j.neuroimage.2018.08.050
37. Smith SM, Beckmann CF, Andersson J, et al. Resting-state fMRI in the Human Connectome Project. *NeuroImage*. 2013;80:144-168. doi:10.1016/j.neuroimage.2013.05.039
38. Harms MP, Somerville LH, Ances BM, et al. Extending the Human Connectome Project across ages: Imaging protocols for the Lifespan Development and Aging projects. *NeuroImage*. 2018;183:972-984. doi:10.1016/j.neuroimage.2018.09.060
39. Zahneisen B, Assländer J, LeVan P, et al. Quantification and correction of respiration induced dynamic field map changes in fMRI using 3D single shot techniques: Respiration Induced Field Map Dynamics. *Magn Reson Med*. 2014;71(3):1093-1102. doi:10.1002/mrm.24771
40. Bancelin D, Bachrata B, Bollmann S, et al. Unsupervised physiological noise correction of functional magnetic resonance imaging data using phase and magnitude information (PREPAIR). *Hum Brain Mapp*. 2023;44(3):1209-1226. doi:10.1002/hbm.26152
41. Kames C, Wiggermann V, Rauscher A. Rapid two-step dipole inversion for susceptibility mapping with sparsity priors. *NeuroImage*. 2018;167:276-283. doi:10.1016/j.neuroimage.2017.11.018
42. Esteban O, Markiewicz CJ, Blair RW, et al. fMRIPrep: a robust preprocessing pipeline for functional MRI. *Nat Methods*. 2019;16(1):111-116. doi:10.1038/s41592-018-0235-4
43. Ostergaard L, Weisskoff RM, Chesler DA, Gyldensted C, Rosen BR. High resolution measurement of cerebral blood flow using intravascular tracer bolus passages. Part I: Mathematical approach and statistical analysis. *Magn Reson Med*. 1996;36(5):715-725. doi:10.1002/mrm.1910360510
44. Ostergaard L, Sorensen AG, Kwong KK, Weisskoff RM, Gyldensted C, Rosen BR. High resolution measurement of cerebral blood flow using intravascular tracer bolus passages. Part II: Experimental comparison and preliminary results. *Magn Reson Med*. 1996;36(5):726-736. doi:10.1002/mrm.1910360511
45. Fisher JA, Venkatraghavan L, Mikulis DJ. Magnetic Resonance Imaging-Based Cerebrovascular Reactivity and Hemodynamic Reserve. *Stroke*. 2018;49(8):2011-2018. doi:10.1161/STROKEAHA.118.021012